Distinct properties underlie flavin-based electron bifurcation in a novel electron transfer flavoprotein FixAB from *Rhodopseudomonas palustris*

Received for publication, October 30, 2017, and in revised form, February 8, 2018 Published, Papers in Press, February 9, 2018, DOI 10.1074/jbc.RA117.000707

H. Diessel Duan[‡], Carolyn E. Lubner[§1], Monika Tokmina-Lukaszewska[¶], George H. Gauss[¶], Brian Bothner[¶], Paul W. King[§1], John W. Peters[‖], and Anne-Frances Miller[‡2]

From the [‡]Department of Chemistry, University of Kentucky, Lexington, Kentucky 40506, the [§]National Renewable Energy Laboratory, Golden, Colorado 80401, the [¶]Department of Chemistry and Biochemistry, Montana State University, Bozeman, Montana 59717, and the [‖]Institute of Biological Chemistry, Washington State University, Pullman, Washington 99163

Edited by Ruma Banerjee

A newly recognized third fundamental mechanism of energy conservation in biology, electron bifurcation, uses free energy from exergonic redox reactions to drive endergonic redox reactions. Flavin-based electron bifurcation furnishes low-potential electrons to demanding chemical reactions, such as reduction of dinitrogen to ammonia. We employed the heterodimeric flavoenzyme FixAB from the diazotrophic bacterium *Rhodopseudomonas palustris* to elucidate unique properties that underpin flavin-based electron bifurcation. FixAB is distinguished from canonical electron transfer flavoproteins (ETFs) by a second FAD that replaces the AMP of canonical ETF. We exploited near-UV–visible CD spectroscopy to resolve signals from the different flavin sites in FixAB and to interrogate the putative bifurcating FAD. CD aided in assigning the measured reduction midpoint potentials ($E°$ values) to individual flavins, and the $E°$ values tested the accepted model regarding the redox properties required for bifurcation. We found that the higher-$E°$ flavin displays sequential one-electron (1-e$^-$) reductions to anionic semiquinone and then to hydroquinone, consistent with the reactivity seen in canonical ETFs. In contrast, the lower-$E°$ flavin displayed a single two-electron (2-e$^-$) reduction without detectable accumulation of semiquinone, consistent with unstable semiquinone states, as required for bifurcation. This is the first demonstration that a FixAB protein possesses the thermodynamic prerequisites for bifurcating activity, and the separation of distinct optical signatures for the two flavins lays a foundation for mechanistic studies to learn how electron flow can be directed in a protein environment. We propose that a novel optical signal observed at long wavelength may reflect electron delocalization between the two flavins.

Electron transfer flavoproteins (ETFs)[3] are found in all domains of life (1). The best-characterized are the canonical ETFs of mammalian mitochondria (2). These serve as a metabolic hub, interacting with and accepting electrons from at least 13 mitochondrial dehydrogenases and conveying electrons to respiratory electron transfer through ETF-ubiquinone oxidoreductase (3). Consistent with ETF's essential role in fatty acid and amino acid metabolism, mutations are often associated with pathogenic phenotypes, such as glutaric acidemia type II in humans (4, 5). Along with the ETFs from bacteria, such as *Paracoccus denitrificans* and *Methylophilus methylotrophus*, these canonical ETFs contain a single FAD as the sole redox center, plus an AMP that plays a structural role, per heterodimer (6–8). However, recent studies have identified a class of ETFs that possess a second FAD instead of the AMP (9, 10) and expand the roles played by this large and ubiquitous flavoprotein family (1).

The first example of a two-FAD–containing ETF came from *Megasphaera elsdenii* (*Mel*ETF), as characterized by Sato *et al.* (11). These authors also provided the initial demonstration of electron acceptance from NADH, in contrast to the canonical ETFs that lack this activity. Thus, the additional FAD in *Mel*ETF was found to accept two electrons from NADH and dispense them one at a time to the other FAD, presumed to correspond to the FAD in canonical ETFs (9). The $E°'$ values determined for *Mel*ETF suggested crossed potentials for the additional FAD, as opposed to the well-separated sequential 1-e$^-$ events displayed by the FAD in canonical ETFs (9). Compelling proposals for the roles for each of the two FADs, as well as a physiological rationale, have emerged from the recent biochemical and crystallographic elucidation of a second two-FAD ETF from *Acidaminococcus fermentans* (*Afe*ETF) (10). This structure demonstrated a protein fold almost superimposable on that of canonical ETFs but containing a second FAD, bound with its AMP portion replacing the AMP of canonical ETFs.

This work was supported as part of the Biological Electron Transfer and Catalysis (BETCy) EFRC, an Energy Frontier Research Center funded by the United States Department of Energy, Office of Science, Basic Energy Sciences, (DE-SC0012518). The authors declare that they have no conflicts of interest with the contents of this article. The content is solely the responsibility of the authors and does not necessarily represent the official views of the National Institutes of Health.

This article contains Figs. S1–S3.

[1] Supported by the United States Department of Energy under Contract DE-AC36-08-GO28308 with the National Renewable Energy Laboratory.

[2] To whom correspondence should be addressed: Dept. of Chemistry, University of Kentucky, Lexington, KY 40506-0055. Tel.: 859-257-9349; E-mail: afmill3r2@gmail.com.

[3] The abbreviations used are: ETF, electron transfer flavoprotein; Bf-FAD, bifurcating FAD; ET-FAD, electron transfer FAD; BCD, butyryl-CoA dehydrogenase; TAS, transient absorption spectroscopy; Bistris propane, 1,3-bis [tris(hydroxymethyl)methylamino]propane; OX, oxidized; HQ, hydroquinone; ASQ, anionic semiquinone; MB, methylene blue; NB, Nile blue; TCEP, tris(2-carboxyethyl)phosphine; PS, phenosafranin; SQ, semiquinone.

The electron-transferring activity of two-FAD ETFs is physiologically profound, as it redistributes the energy embodied by NADH's reducing power *unequally* among the two electrons transferred. This is accomplished by a fundamental mechanism of biological energy conservation, known as electron bifurcation (12). In the case of *Afe*ETF, one of the FADs accepts electrons from NADH ($E^{\circ\prime} = -320$ mV) (13) and delivers them to two distinct acceptors, one at high potential (exergonic electron transfer causing the reaction to be favorable overall) and the other at lower potential (endergonic electron transfer capturing and conserving excess energy) (10). Hence, we refer to this flavin as the putative bifurcating flavin (Bf-FAD). Under the proposed mechanism, each round of bifurcation passes one electron from the Bf-FAD to the other FAD in *Afe*ETF (herein called the electron transfer FAD, ET-FAD) and the other electron to ferredoxin ($E^{\circ\prime} = -420$ mV) (14). The ET-FAD is proposed in turn to reduce crotonyl-CoA to butyryl-CoA ($E^{\circ\prime} = -10$ mV) via butyryl-CoA dehydrogenase (BCD), thereby "paying for" the endergonic reduction of ferredoxin (10).

This elegant coupling of exergonic and endergonic redox reactions mediated by a flavin cofactor conserves energy in the form of reduced ferredoxin or flavodoxin (15) that can serve as electron donors for nitrogen fixation (1). Indeed, homologs of these bifurcating ETFs, termed FixABs due to their functional linkage to nitrogen fixation, have been identified in a variety of diazotrophic bacteria, such as *Rhodopseudomonas palustris*, *Azotobacter vinelandii*, and *Rhodospirillum rubrum* (1, 16–18). Furthermore, it has been shown that disruption of the Fix complex, FixABCX, abrogates cell growth in *R. palustris* under nitrogen-fixing conditions and lowers cellular nitrogenase activity by some 75% in *R. rubrum* (16, 18). More recently, the FixABCX complex of *A. vinelandii* has been demonstrated to bifurcate electrons from NADH to generate flavodoxin hydroquinone and reduced quinone, similar to the ETF-BCD systems of *A. fermentans* and *M. elsdenii* (19). However, a detailed study of the Fix complex has been hampered by the difficulty of producing high-quality preparations in the quantities needed for biochemical and biophysical characterizations.

We now describe the FixAB component of FixABCX from *R. palustris* (*Rpa*FixAB) that is hypothesized to bifurcate electrons to generate reduced ferredoxin for nitrogenase (16). Given the prodigious metabolic versatility of *R. palustris*, it makes sense that the organism employs a member of the ETF family already well-established as a means of interfacing different electron donors and acceptors. Moreover, the fact that *Afe*ETF reduces both ferredoxin and flavodoxin, which can themselves be donors to diverse metabolic processes, suggests that bifurcating ETFs in general may act as versatile low-potential electron providers.

Given that capacity to execute the novel activity of bifurcation is associated with possession of a second FAD in lieu of the AMP found in canonical ETFs, the additional flavin is a strong candidate for the site of bifurcation. In order to evaluate this hypothesis and elucidate crucial tenets of flavin-based bifurcation, we have purified FixAB from *R. palustris* with a full complement of 2 FADs/heterodimer, demonstrated a spectroscopic means of distinguishing the two flavins, and measured E° values for each of them. We have thereby tested two central mechanistic criteria for bifurcation: 1) that the Bf-FAD be unstable as a semiquinone and therefore display a single 2-e$^-$ E° in titrations and 2) that FixAB should possess a means of extracting one electron from reduced Bf-FAD to produce a transient semiquinone in the course of turnover.

Results

Purification and flavin content of RpaFixAB

Recombinant FixAB with two His tags was purified to homogeneity as assessed by SDS-PAGE (Fig. 1*A*) with typical yields of 2 mg protein/liter of culture. The protein was reconstituted to full flavin occupancy (*i.e.* 2 FADs/heterodimer in Tris, pH 7.8), as demonstrated by quantification of released FAD (2.1 ± 0.2, $n = 3$ determinations, Fig. 1*B*). The flavin content was corroborated by native mass spectrometry. The protein heterodimer mass matched the expected mass for a complex containing two FADs, but not the mass expected for a complex containing one FAD and one AMP (Fig. 1*C*), confirming that *Rpa*FixAB contains two FAD molecules as opposed to the cofactor content observed for canonical ETFs.

The absorption spectrum of *Rpa*FixAB reveals relatively subtle perturbation of the two flavins (Fig. 1*B*). Compared with free FAD at pH 7.8, the lower energy transition was red-shifted from 450 to 454 nm, and the higher-energy transition was red-shifted from 375 to 380 nm. The ratio of A_{454} *versus* A_{380} was 1.04 in *Rpa*FixAB *versus* $A_{450}/A_{375} = 1.24$ in free FAD, accompanied by a red shift of the trough from 404 to 410 nm. Interestingly, a charge-transfer band (520–620 nm) was observed that has not been reported previously for any ETF. We hypothesize that it represents a flavin-thiolate interaction between the Bf-FAD and the nearby side chain of Cys-174 from FixB (20, 21). This Cys is conserved among all 55 Fix sequences compared, suggesting that the optical feature will also be present in other FixAB complexes. However, this Cys is replaced by Ala in the *Afe*ETF, explaining the absence similar long-wavelength absorbance from its oxidized (OX) state spectra (10).

Circular dichroism deconvolution of the two flavins in RpaFixAB

Whereas the optical signals of the two flavins are heavily overlapped, CD has the crucial advantage that signals can have different signs and amplitudes while still occurring at the same wavelength. Bound flavins have been observed to display very different CD signals, depending on their binding sites (22–25). We exploited this added sensitivity to local environment to obtain distinct spectral signatures for each of *Rpa*FixAB's two flavins.

To test the capacity of CD to resolve optical features of the two different flavins, we prepared *Rpa*FixAB depleted with respect to the putative ET-FAD by competition with ATP. ATP was shown to bind to the FAD site of (canonical) porcine ETF in competition with FAD, whose FMN component was found to not contribute to the free energy of binding (26). Similarly, the counterpart of ET-FAD in the two-FAD–containing *Mel*ETF is more weakly bound to the protein than the putative Bf-FAD (11); thus, we expect that ET-FAD would be displaced first by ATP. To optimize the selectivity of the displacement, we did not seek to fully deplete one FAD site (9, 11), as very high ATP

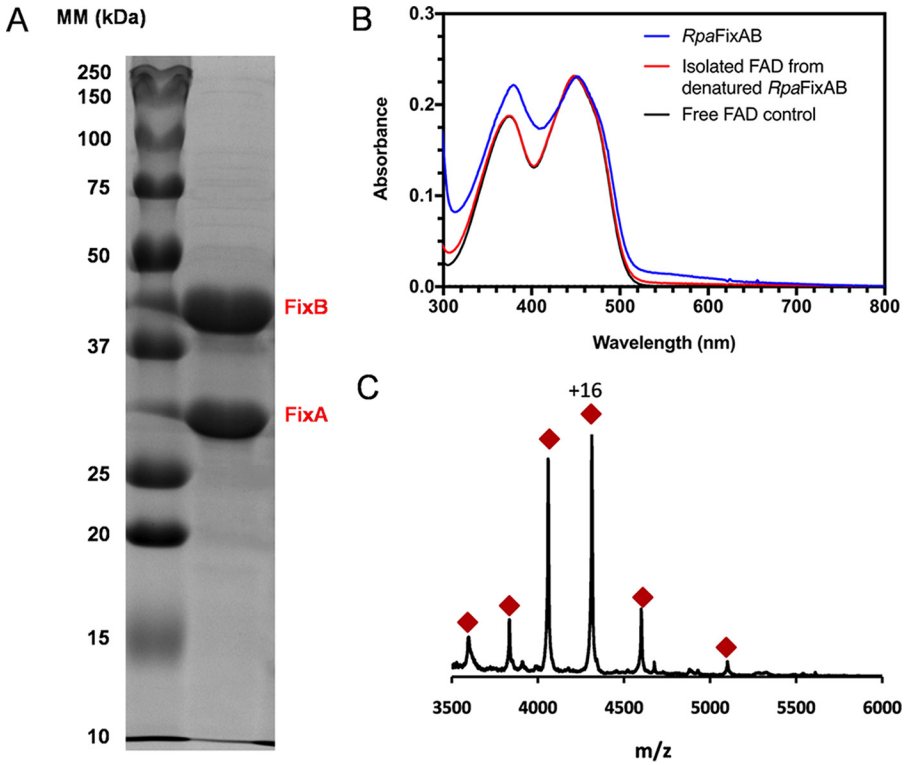

Figure 1. *A*, SDS-PAGE of purified His-tagged *Rpa*FixAB (*right lane*). Pure FixA and FixB isolated from inclusion bodies were used as controls shown in the marker lane (*left lane*). *B*, UV-visible spectrum of 8.6 μM *Rpa*FixAB with full flavin occupancy in 20 mM Tris, pH 7.8, 200 mM KCl, 10% glycerol (w/v), and 1 mM TCEP compared with free FAD. *C*, native mass spectrum of *Rpa*FixAB containing two FAD cofactors determined with 0.5 μM protein in 200 mM ammonium acetate, pH 7.0. *Red diamonds* denote charge state envelope centered around a charge of +16. The experimental mass of *Rpa*FixAB is 76,194 Da, compared with the predicated mass of 76,195 Da for protein containing two FADs and 75,755 Da for protein containing one FAD and one AMP.

concentrations or more extensive FAD depletion produces protein aggregation at the concentration required for near-UV–visible CD experiments. However CD offers the advantage that displaced FAD in solution makes a negligible contribution to the CD spectra, consistent with the planarity of the isoalloxazine ring system (Fig. S1).

Whereas the absorption spectrum displayed only subtle changes accompanying release of FAD from the presumed ET-FAD site, the CD spectrum changed markedly (Fig. 2). We interpret the difference CD spectrum (*blue* in Fig. 2*B*) as the CD signature of preferential depletion of one FAD site as opposed to loss of FAD from both sites, because comparable FAD losses from both sites would not be expected to change the shape of the CD spectrum, only its amplitude. Based on the analogy with porcine and *Mel*ETF, the site that was depleted is the ET-FAD site. Thus, the difference spectrum between the starting spectrum at 0 mM ATP and the end spectrum at 13 mM ATP is deduced to be the CD signature of the putative ET-FAD (Fig. 2*B*), although at substoichiometric amplitude.

To test the identity of the flavin displaced by ATP and thus the attribution of the CD signature, we also recorded CD spectra of *Rpa*FixAB as a function of stepwise reduction by NADH or sodium dithionite. If the difference spectrum in Fig. 2*B* indeed represents the ET-FAD, then the difference CD spectrum (OX minus half-reduced) should be similar, because the first CD signature silenced upon reduction should be that of the ET-FAD. In support, ET-FAD is proposed to accept electrons from Bf-FAD and therefore must have higher E° values (9), and the FAD of canonical ETFs (corresponding to Fix ET-FAD) has considerably higher E° values than the additional FAD of bifurcating ETFs (presumed Bf-FAD) (27–29).

Data from reduction with NADH are shown in Fig. 3, and the results from dithionite reduction were essentially the same. Upon reduction to the hydroquinone (HQ) state, FAD becomes a much weaker chromophore in the visible range, and its CD signature is likewise attenuated; therefore, stepwise reduction of FixAB silences the flavin with the higher E° first and then silences the lower-E° flavin. The optical spectra obtained in the course of stepwise anaerobic reduction of *Rpa*FixAB by NADH showed that half of the FAD population underwent reduction via an anionic semiquinone (ASQ) state manifested by increased absorbance at 376 and 550–600 nm *en route* to HQ (at one equivalent of NADH). Thus, we conclude that one of the two FADs undergoes sequential 1-e^- reductions (Figs. 3 (*A* and *B*) and 5). We identify this higher-E° FAD with the ET-FAD by analogy with canonical ETFs from humans and pigs (30–32). At the point when the ET-FAD is fully reduced but the Bf-FAD is still oxidized, the CD spectrum is distinct from the starting spectrum, confirming that reduction has affected the two sites unequally (Fig. 3*C*). Subtraction of the spectrum of this semireduced *Rpa*FixAB from that of fully oxidized *Rpa*FixAB yields a difference CD signal that should correspond to ET-FAD (*blue* in Fig. 3*C*). Comparison with the one obtained via displacement with ATP reveals excellent agreement (*blue* in Fig. 2*B*), showing that the FAD displaced by ATP is the one with the higher E° and therefore corresponds to the ET-FAD based on two independent criteria. It follows that the other CD component, collected

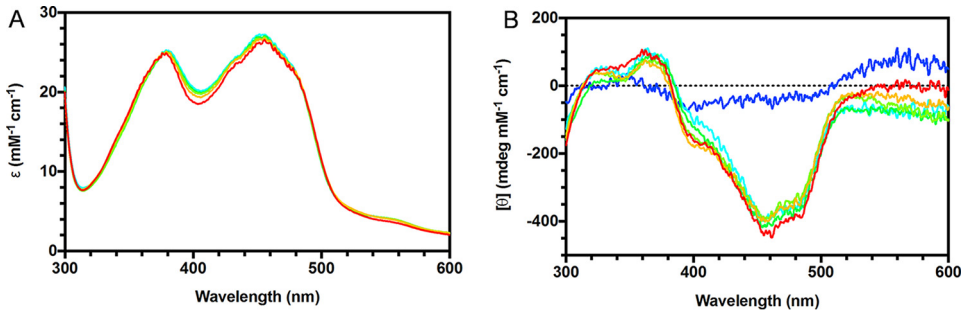

Figure 2. *A*, UV-visible spectra of 65 μM *Rpa*FixAB with its FAD displaced by 0 mM (*red*), 3.25 mM (*orange*), 6.50 mM (*lime*), 9.75 mM (*green*), and 13.00 mM (*cyan*) ATP in 20 mM Bistris propane, pH 9.0, 200 mM KCl, 10% glycerol (w/v), and 1 mM TCEP at 4 °C. *B*, near-UV–visible CD spectra of 65 μM *Rpa*FixAB with its FAD displaced by 0 mM (*red*), 3.25 mM (*orange*), 6.50 mM (lime), 9.75 mM (*green*), and 13.00 mM (*cyan*) ATP in 20 mM Bistris propane, pH 9.0, 200 mM KCl, 10% glycerol (w/v), and 1 mM TCEP at 4 °C. The *blue spectrum* is the difference spectrum obtained by subtraction of the cyan spectrum dominated by the putative Bf-FAD from the red spectrum made up of both Bf-FAD and ET-FAD, demonstrating CD signal attributed to the ET-FAD.

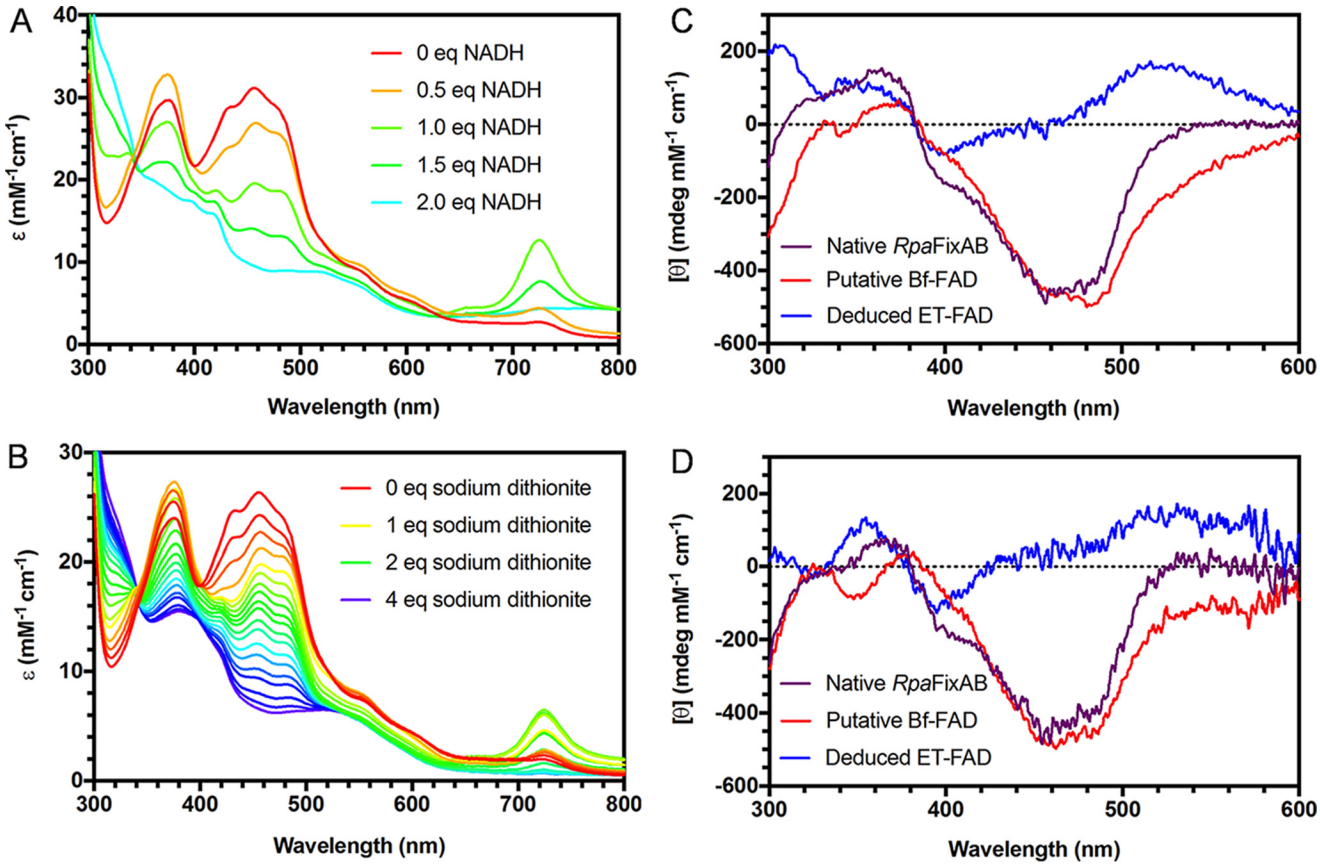

Figure 3. *A* and *B*, UV-visible spectra of 65 μM *Rpa*FixAB reduced by stepwise additions of 32.5 μM NADH at 4 °C (*A*) or 14.5 μM sodium dithionite at room temperature (*B*) in 20 mM Bistris propane, pH 9.0, 200 mM KCl, 10% glycerol (w/v), and 1 mM TCEP. Near-UV–visible CD spectra of the putative Bf-FAD at 1 eq of NADH at 4 °C (C) and 2 eq of sodium dithionite at room temperature (*D*) are shown in *red* in 20 mM Bistris propane, pH 9.0, 200 mM KCl, 10% glycerol (w/v), and 1 mM TCEP. The *purple spectra* in both *C* and *D* are the native *Rpa*FixAB CD spectra composed of both Bf-FAD and ET-FAD. The *blue spectrum* is the difference spectrum obtained by subtraction of the red spectrum of the putative Bf-FAD from the purple spectrum made up of both putative Bf-FAD and ET-FAD, demonstrating the CD spectrum of the ET-FAD in both *C* and *D*.

as the spectrum of semireduced *Rpa*FixAB, must correspond to the other FAD: the putative Bf-FAD.

To test whether the sequence of reductions reflected the identity of the reductant or could be interpreted in terms of simple thermodynamic ease of reduction, we also characterized the effects of stepwise reduction by the 1-e^- donor sodium dithionite. This donor has been shown to reduce the FAD of canonical ETFs to form ASQ and then HQ (33). The same was observed with *Rpa*FixAB for the first of the two FADs to be reduced. As demonstrated in Fig. 3*D*, reduction of *Rpa*FixAB by 2 eq of sodium dithionite produced a CD spectrum resembling that of Bf-FAD observed halfway through stepwise reduction with NADH, showing loss of the inflection near 380 nm attributed above to ET-FAD as well as the positive CD at wavelengths larger than 500 nm. These data confirm the difference CD signature to be that of ET-FAD as well as the three sequential redox reactions (9) (Fig. 4*A*).

*Rpa*FixAB is rapidly reduced by NADH, which does not reduce canonical ETFs (9, 10, 34). This is understood to be the result of electron transfer from NADH to the Bf-FAD, which is

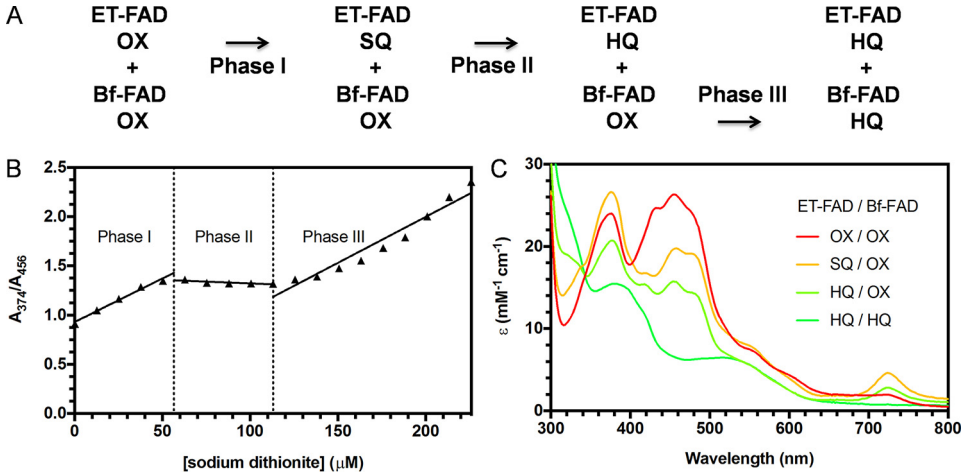

Figure 4. *A*, sequential reduction of ET-FAD and Bf-FAD of *Rpa*FixAB: 1-e$^-$ reduction of ET-FAD (Phase I and II) and 2-e$^-$ reduction of Bf-FAD (Phase III). *B*, summary of spectral changes accompanying reduction of 65 μM *Rpa*FixAB by sodium dithionite at room temperature in 20 mM Bistris propane, pH 9.0, 200 mM KCl, 10% glycerol (w/v), and 1 mM TCEP resolved into three phases by linear fits of A_{374}/A_{456} *versus* dithionite concentration, yielding different slopes for each phase. *C*, initial and final spectra for each phase of reduction of 65 μM *Rpa*FixAB at room temperature in 20 mM Bistris propane, pH 9.0, 200 mM KCl, 10% glycerol (w/v), and 1 mM TCEP, with dithionite as the reductant.

not present in canonical ETFs. Accordingly, dithionite reduced the Bf-FAD by 2-e$^-$ without accumulation of semiquinone (Fig. 3, *A* and *B*). Thermodynamic suppression of the semiquinone state has been proposed to represent a hallmark of a bifurcating site (12, 35, 36) and therefore is examined in further detail below.

Even upon full reduction, we retained a broad optical feature near 400 and 540 nm that was not reduced by additional NADH or dithionite. We speculate that this may represent a conformation that is kinetically trapped in the ASQ state as in *M. methylotrophus* ETF (29). Another possibility is charge transfer from a reduced flavin (37, 38) to a nearby cation, such as Arg-165.

An intriguing optical signature associated with partially reduced RpaFixAB

Incomplete reduction by NADH produced a spectral feature that was also present although less prominent upon partial reduction with dithionite (Fig. 3, *A* and *B*). A sharp band centered at 726 nm accumulated and then disappeared in the course of reduction. Its intensity was maximal when ~1 eq of NADH had reacted, suggesting that it may represent a charge-transfer species involving the two flavins. It is not typical of flavin charge-transfer bands described in other systems, which tend to have shorter wavelength absorption maxima and much larger line widths (20, 37, 39–41). The 726-nm species is formed when dithionite is the titrant and so would have to represent a co-purifying nicotinamide if a charge-transfer band with it were to be proposed (42). However, ET-FAD$_{HQ}$·NAD$^+$ is unlikely, given that NADH appears not to interact with the ET-FAD, and ET-FAD$_{HQ}$ would persist through the end of the titration. The Bf-FAD is known to interact with nicotinamides but would be oxidized midway through the titration, requiring that the interaction represent Bf-FAD$_{OX}$·NADH, which should react rather than accumulate. Because this signal grows as the ET-FAD is reduced but disappears as the Bf-FAD is reduced, it appears that the species' formation depends on the oxidation states of both flavins, not just one of them. Therefore, we speculate that the 726-nm species represents delocalized charge transfer between the two flavins, for example mediated by the adenine ring and intervening Tyr-37 (43) as discussed below.

Reduction midpoint potentials of the two flavins in RpaFixAB

Optically monitored titrations of *Rpa*FixAB enabled us to determine $E°$ values for the redox couples associated with the three phases of reduction observed by titration with dithionite or NADH. By using the xanthine/xanthine oxidase electron delivery system (44) and repeating the experiment in the presence of a series of reference dyes chosen to buffer the system in different redox regimes (45), we determined the $E°$ values of both flavins and evaluated the hypothesis that the Bf-FAD should have crossed potentials (12, 35, 36). To resolve the three phases of the redox titration, the ratio of absorption intensity at 374 nm (where ASQ is stronger) and 456 nm (where OX is stronger) was evaluated as a function of reductant concentration (Fig. 4*B*) (46). Three phases were characterized by distinct slopes, justifying interpretation of the data in terms of three sequential reduction events. Fig. 4*C* provides the spectra corresponding to the junctures between the phases and confirms that these points in the titration are dominated by the species indicated in Fig. 4*A*.

For the first (most positive) redox couple in which ET-FAD is reduced from the OX state to ASQ, concurrent reduction of flavin and methylene blue (MB) (47) was observed with increased absorbance at 374 nm (ASQ) and decreased absorbance at 456 nm (32) in addition to decreased absorbance at 664 nm due to conversion of the oxidized MB chromophore to non-absorbing reduced MB (Fig. 5). The change in absorbance at 456 nm (ΔA_{456}) was taken to represent loss of OX and formation of ASQ. The difference extinction coefficient at 456 nm corresponding to reduction was calculated from extrema spectra ($\Delta\epsilon_{456}$, from the spectrum of fully OX ET-FAD minus the spectrum containing the largest amount of ASQ ET-FAD) and then used to calculate the concentration of ET-FAD$_{SQ}$ at each point in the titration, assuming conversion of 1.0 ET-FAD$_{OX}$.

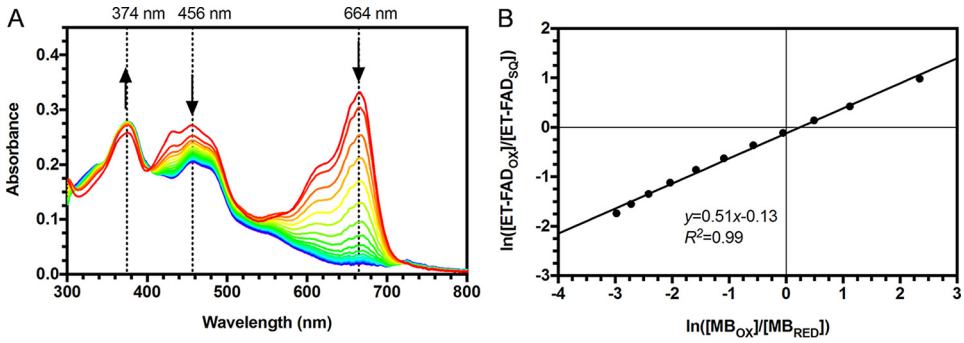

Figure 5. *A*, co-reduction of ET-FAD (OX to SQ) and MB by xanthine/xanthine oxidase in 20 mM Bistris propane, pH 9.0, 200 mM KCl, 10% glycerol (w/v), and 1 mM TCEP. *Arrows* indicate the direction of the absorbance change at the wavelength monitored every 1 min for 1–2 h. The concentration of oxidized MB was monitored at 664 nm, and the concentrations of ET-FAD$_{OX}$ and ET-FAD$_{SQ}$ were monitored at 456 nm with three independent titrations performed. *B*, linear best fit of ln([ET-FAD$_{OX}$]/[ET-FAD$_{SQ}$]) *versus* ln([MB$_{OX}$]/[MB$_{RED}$]) used for calculation of the $E°$.

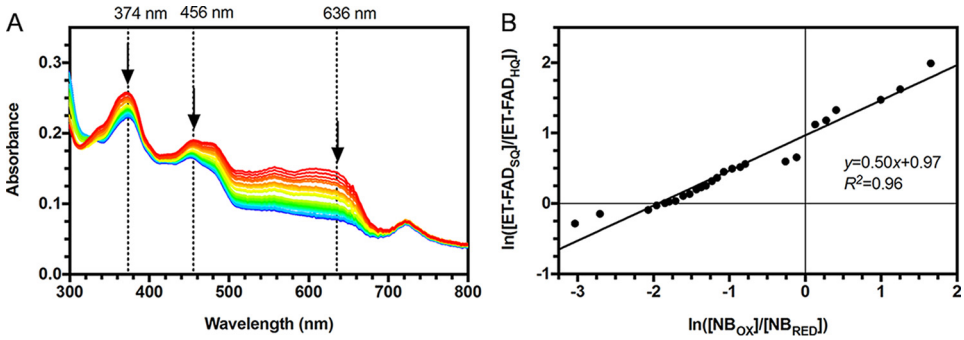

Figure 6. *A*, co-reduction of ET-FAD (SQ to HQ) and NB by xanthine/xanthine oxidase in 20 mM Bistris propane, pH 9.0, 200 mM KCl, and 10% glycerol (w/v). *Arrows*, direction of the absorbance change at the wavelength monitored every 1 min for 1–2 h. The concentration of oxidized NB was monitored at 636 nm, and the concentrations of ET-FAD$_{SQ}$ and ET-FAD$_{HQ}$ were monitored at 456 nm with three independent titrations performed. *B*, linear best fit of ln([ET-FAD$_{SQ}$]/[ET-FAD$_{HQ}$]) *versus* ln([NB$_{OX}$]/[NB$_{RED}$]) used for calculation of the $E°$.

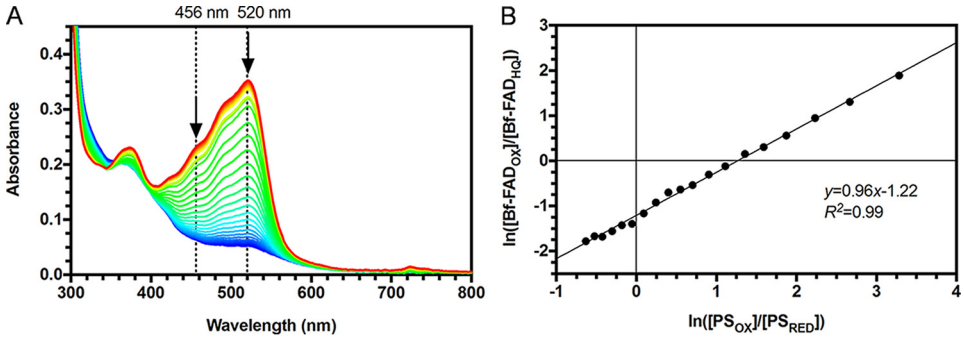

Figure 7. *A*, co-reduction of Bf-FAD (OX to HQ) and PS by xanthine/xanthine oxidase in 20 mM Bistris propane, pH 9.0, 200 mM KCl, 10% glycerol (w/v), and 1 mM TCEP. *Arrows*, direction of the absorbance change at the wavelength monitored every 1 min for 1–2 h. The concentration of oxidized PS was monitored at 520 nm, and the concentrations of Bf-FAD$_{OX}$ and Bf-FAD$_{HQ}$ were monitored at 456 nm with three independent titrations performed. *B*, linear best fit of ln([Bf-FAD$_{OX}$]/[Bf-FAD$_{HQ}$]) *versus* ln([PS$_{OX}$]/[PS$_{RED}$]) used for calculation of the midpoint potential.

A plot of ln([ET-FAD$_{OX}$]/[ET-FAD$_{SQ}$]) *versus* ln([MB$_{OX}$]/[MB$_{RED}$]) resulted in a slope of 0.51 (Fig. 5*B*), which is in agreement with the theoretical value of 0.5 expected for 1-e$^-$ reduction of FAD *versus* 2-e$^-$ reduction of MB (see Equation 1) (44). From the intercept of the line, an $E°$ of −47 ± 4 mV (pH 9.0, n = 3 determinations) was obtained for the ET-FAD OX/ASQ couple ($E°_{\text{ET-FAD, OX/ASQ}}$) *versus* an $E°$ of −49 mV for MB at this pH (Fig. 5 and Equation 2). The positive slope relating the ratio of A_{374}/A_{456} to the reduction coordinate confirms that Phase I reduction indeed corresponds to conversion of OX flavin to ASQ (Fig. 4*B*).

The $E°_{\text{SQ/HQ}}$ of the ET-FAD (*i.e.* $E°_{\text{ET-FAD, SQ/HQ}}$) was determined using Nile blue (NB) (31) as the reference dye (Fig. 6*A*). The disulfide bond reducing agent tris(2-carboxyethyl)phosphine (TCEP) was removed from samples used for these titrations because it was found to react with Nile blue (data not shown). The slope of 0.50 from the ln/ln fit matches the theoretical value and indicates 1-e$^-$ reduction of FAD *versus* 2-e$^-$ reduction of NB (Fig. 6*B*). The plot of A_{374}/A_{456} *versus* the reduction coordinate displayed a zero slope, further confirming the nature of Phase II reduction as conversion of ASQ to HQ (Fig. 4*B*), because this conversion causes absorbance to decrease similarly at both of those wavelengths. The measured $E°_{\text{ET-FAD, SQ/HQ}}$ was −203 ± 3 mV (pH 9.0, n = 3 determinations, *versus* an $E°$ of −236 mV for NB at this pH) (Fig. 6), confirming separation between the two $E°$ values of ET-FAD, as indicated by the accumulation of stable ET-FAD ASQ at intermediate potentials (supplemental Fig. S2*A*).

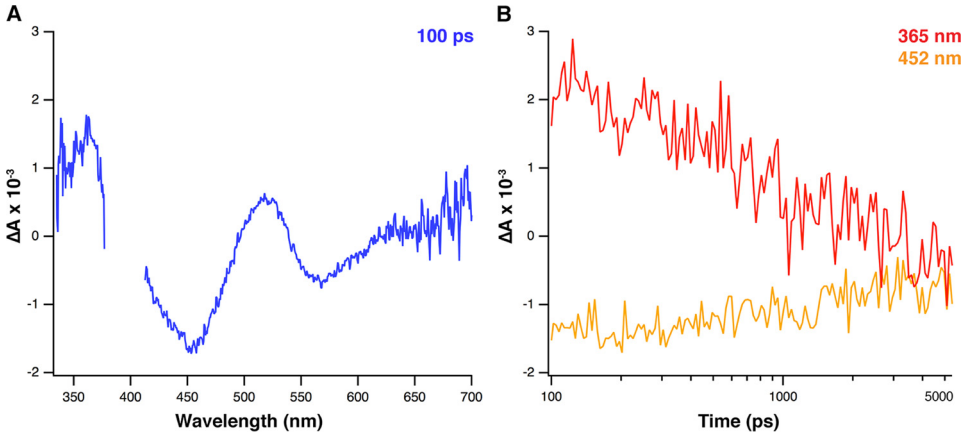

Figure 8. *A*, UV-visible difference absorption spectrum showing transient formation of ASQ in *Rpa*FixAB 100 ps after photoexcitation. *B*, kinetic traces of its reoxidation to OX flavin as observed via decay of difference absorbance at 365 nm (ASQ) and recovery from bleach at 452 nm (OX). See "Results" for details; note that the *vertical axes* for difference absorption are in milliabsorbance units, such that a value of 3 indicates a change in absorbance of 0.003, and also that the vertical location of $\Delta A = 0$ is not known with certainty, as the long-wavelength data can include negative as well as positive contributions and therefore can only give a rough estimate of the location of $\Delta A = 0$.

Concomitant reduction Bf-FAD and phenosafranin (PS) enabled determination of the $E°$ of Bf-FAD, associated with the Phase III reduction (Fig. 7). The optical changes indicated that this event corresponds to reduction of FAD from the OX to the HQ state. A slope of 1.09 from the best linear fit of ln([Bf-FAD_{OX}]/[Bf-FAD_{HQ}]) *versus* ln([PS_{OX}]/[PS_{RED}]) agreed well with the theoretical value of 1 anticipated for 2-e^- reduction of Bf-FAD and 2-e^- reduction of PS (Fig. 7*B*). An $E°$ of -283 ± 3 mV (pH 9.0, $n = 3$ determinations, *versus* an $E°$ of -312 for PS at this pH) was obtained for Bf-FAD consistent with its capacity to accept electrons from NADH. A positive slope from the plot of A_{374}/A_{456} *versus* the reduction coordinate verified the conversion of OX to HQ in Phase III because the HQ formed absorbs near 374 nm but not near 456 nm.

Detection of short-lived flavin species by transient absorption spectroscopy

TAS has succeeded in revealing flavin intermediates with picosecond lifetimes in other bifurcating enzymes (1, 47, 48). In TAS, flavin ASQ is generated via photoexcitation of oxidized flavin, which then abstracts an electron from nearby electron donors, such as Trp or Tyr residues, or reduced cofactors (49, 50). Transient absorption attributable to ASQ was indeed observed in difference spectra of *Rpa*FixAB (photoexcited minus non-photoexcited; Fig. 8*A*). Clear positive ΔA in the ranges of 350–400 and 500–550 nm in conjunction with equally strong negative ΔA in the range of 410–480 nm are consistent with formation of ASQ at the expense of OX, 100 ps after photoexcitation (48). Negative ΔA at wavelengths longer than 540 nm can represent emission from photoexcited OX flavin (51, 52). In our case, an additional source of this negative signal can be conversion of OX Bf-FAD to the ASQ form in so far as the OX state of Bf-FAD has charge-transfer absorbance intensity in this region that will be lost upon flavin reduction (Fig. 1*B*). The strength of this feature argues that both of the foregoing contribute.

Fig. 8*B* shows the subsequent evolution of the system. From 100 ps onward the trajectories reveal recovery of OX coincident with decay of ASQ indicative of electron transfer from ASQ back to the oxidized donor to regenerate OX flavin, because our *Rpa*FixAB dimer lacks other electron transfer partners. The decay of ASQ difference absorption is best fit by a double-exponential model with half-lives of 380 ± 50 and 3000 ± 500 ps, each representing 50% ± 2% of the population. The two half lives could reflect conformational heterogeneity. However, given that both have considerable amplitude, it is simplest to consider that they reflect the two flavins and thus that even the Bf-FAD forms ASQ. The capacity of this system to produce a transient ASQ Bf-FAD satisfies a fundamental requirement for bifurcating activity (47, 48).

Discussion

Although it is well-established that the canonical ETFs contain 1 FAD and 1 AMP per heterodimer, the recent reports of ETFs with two FADs, such as *Mel*ETF, have highlighted concern over discrepancies among preparations regarding either low flavin occupancy or presence of modified flavins (11). However, Sato *et al.* (9) and Chowdhury *et al.* (34) achieve 1.8–1.9 FADs per ETF heterodimer with no reported modified flavins for *Mel*ETF purified after homologous and heterologous expression, respectively. The new *Rpa*FixAB ETF characterized in our studies is unique in that this two-FAD–containing ETF has been linked to nitrogenase function (1) and shown to be essential for *R. palustris* growth under nitrogen-fixing conditions (16). The flavin absorption spectrum of *Rpa*FixAB exhibits notable differences from other bifurcating ETFs. It lacks the unusual absorption centered around 400 nm seen in *Mel*ETF and attributed to "FAD-2" (here called ET-FAD) (11). A similar feature was also reported from the bifurcating *Afe*ETF (10); however, it is absent in our *Rpa*FixAB and also from the *Mel*ETF characterized by Chowdhury (34). Unlike *Mel*ETF studied by Chowdhury *et al.* (34), both the 380 and 454 nm bands of *Rpa*FixAB at pH 7.8 were 4–5 nm red-shifted relative to those of free FAD, and their intensity difference became less prominent at pH 7.8, which is also distinct from free FAD.

Reduction of *Rpa*FixAB by either NADH, sodium dithionite, or the xanthine/xanthine oxidase system occurred in three distinct phases, as for *Mel*ETF (9). An optical signal reminiscent of

Table 1
Redox potentials of characterized ETFs measured at pH 7.0 or adjusted to pH 7.0

System	Organism	Flavin content	$E^{\circ\prime}$ OX/ASQ; ASQ/HQ; OX/HQ	Reference
			mV	
Free flavin	NA[a]	NA	−313; −101; −207	Ref. 57[b]
Two-FAD ETFs				
FixAB	*R. palustris*	2	−47; −83; −223	This study[c]
ETF	*M. elsdenii*	2	+81; −136; −279	Ref. 9
One-FAD ETFs				
ETF	*Homo sapiens*	1	+37; +25; NA	Ref. 23
			+22; −42; NA	Ref. 52
ETF	*Sus domesticus*	1	−14; −30; NA	Ref. 45[d]
			+4; −20; NA	Ref. 31[e]
ETF	*P. denitrificans*	1	−6; −36; NA	Refs. 50 and 51[f]
ETF	*M. methylotrophus*	1	+196; −197; NA	Ref. 26
			+141; NA; NA	Ref. 27
			+153; <−250; NA	Ref. 28

[a] NA, not applicable, as the affected flavin is not present.
[b] Free FMN at pH 7.0; neutral semiquinone is formed in contrast to the situation in ETF and Fix.
[c] E° values measured at pH 9.0. Tabulated $E^{\circ\prime}$ values calculated from E° values as described under "Experimental procedures."
[d] Measurements were made at pH 7.1, and tabulated values were adjusted as described under "Experimental procedures."
[e] Measurements were made at pH 7.5, and tabulated values were adjusted as described under "Experimental procedures."
[f] Measurements were made at pH 7.4, and tabulated values were adjusted as described under "Experimental procedures."

anionic semiquinone but shifted to longer wavelengths remains visible in the presence of excess reductants when no mediators are present. Such behavior was also documented for the ETF of *M. methylotrophus*, wherein it was explained as the result of conformational heterogeneity in which one conformation was kinetically impeded from undergoing full reduction (29). As in that case, we find that this feature is suppressed by the presence of mediators, which allow full reduction (see Fig. 7*A*).

The unique band we observe at 726 nm is unprecedented to our knowledge and seems to correlate with HQ ET-FAD in the presence of OX Bf-FAD. It is unique in being much sharper than typical charge-transfer bands reported in flavoenzymes (53). This band forms regardless of the means employed to reduce the system, so we conclude that it represents components inherent to the *Rpa*FixAB protein. Because its appearance correlates with partial reduction of the system as a whole rather than the state of either flavin alone, we speculate that it represents long-range charge delocalization between the flavins (*e.g.* mediated by the adenine ring of the Bf-FAD and the conserved Tyr between it and the ET-flavin). Although the total separation between flavins is 18 Å, such a species has been documented, mediated by a Trp residue between hemes 14.5 Å apart in MauG (43). Raman spectroscopy combined with *ab initio* density functional theory calculations are under way to unravel the chemical identity of this species.

Our CD deconvolutions by two different approaches unequivocally demonstrate that the two FADs present in *Rpa*FixAB experience distinct environments as revealed by distinct CD spectra. No other visible CD characterization of the Bf-FAD has yet been reported, but our deduced ET-FAD CD spectra resemble the CD signature of its counterpart FAD from *M. methylotrophus* ETF, although both bands are substantially red-shifted in *Rpa*FixAB (54). These results suggest a more polar environment for the ET-FAD in *Rpa*FixAB. The contrasting spectral signatures of the two FADs, not available via absorption spectra, yield information about the flavin environments and facilitate attribution of chemical events to individual flavins, thus setting the stage for detailed mechanistic studies.

The E° values determined in our studies conform to the hypothesis that crossed potentials should be required for the Bf-FAD (35). Little if any semiquinone of Bf-FAD accumulates in reductions by NADH, dithionite, or xanthine/xanthine oxidase. This is consistent with the slope within error of unity for the ln/ln plot (Fig. 7*B*). The redox reactivity of the Bf-FAD is thus qualitatively distinct from that of the ET-FAD but in agreement with mechanistic proposals for bifurcating activity.

Reduction of the ET-FAD proceeds via sequential 1-e$^-$ reductions with a prominent ASQ intermediate similar to the behavior of all canonical ETFs for which we could find reports, as well as the corresponding "FAD-2" or "α-FAD" in *Mel*ETF and *Afe*ETF, respectively, although the ASQ feature of ET-FAD is less prominent in Chowdhury's work on *Mel*ETF and *Afe*ETF. The E° values published for various ETFs are tabulated in Table 1, adjusted to pH 7.0 (24, 27–32, 55, 56). *Rpa*FixAB appears to have a much lower $E^{\circ\prime}$ for the ET-FAD OX/ASQ couple than the other ETFs. This could reflect the presence of a conserved Glu near ET-FAD in *Rpa*FixAB *versus* a conserved Lys in *Mel*ETF (conserved as Lys in 50 of 81 Group 2A ETF sequences aligned (1)) and a conserved Arg in all but 6 of 473 Group 1 ETFs aligned including human, porcine, and *P. denitrificans* ETF (Table 1). Replacement of a positive charge with a negative charge is expected to disfavor formation of the ASQ on electrostatic grounds and is thus consistent with *Rpa*FixAB's considerably lower $E^{\circ}_{\text{ET-FAD, OX/ASQ}}$. The Glu in *Rpa*FixAB is Glu in 52 of 55 FixA sequences aligned and Asp in the remaining 3 (1), so we anticipate that the other FixAB complexes will also have a relatively low $E^{\circ}_{\text{ET-FAD, OX/ASQ}}$. However, we also note that *Rpa*FixAB's E° was measured at a higher pH than the others in Table 1, and the tabulated $E^{\circ\prime}_{\text{ET-FAD, OX/ASQ}}$ value assumes that no proton is taken up upon flavin reduction. Our spectra show that the flavin itself does not acquire a proton, but if a nearby amino acid acquires a proton in conjunction with ASQ formation, the $E^{\circ\prime}_{\text{ET-FAD, OX/ASQ}}$ could be as high as 73 mV, in much better agreement with the value of 81 mV for the two-FAD–containing *Mel*ETF. *Rpa*FixAB does not tolerate

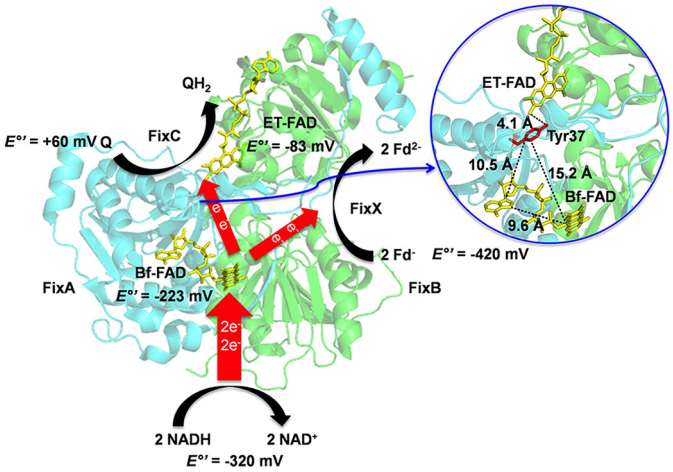

Figure 9. Proposed mechanism of electron bifurcation for the Fix system, illustrated on the structure of the homologue *Afe*ETF. The *enlargement* in the *circle* shows Tyr-37 possibly involved in interflavin electron transfer and the distances between it and the two FADs. The distance between ET-FAD and Tyr-37 is 4.1 Å. The distance between Tyr-37 and the isoalloxazine ring of Bf-FAD is 15.2 Å. However, considering the adenine ring of Bf-FAD as an electron-hopping site, the distance between Tyr-37 and adenine of Bf-FAD is only 10.5 Å, and the distance between the adenine and the flavin of Bf-FAD is 9.6 Å (shortest distances between non-hydrogen atoms). Coordinates from the structure of *Afe*ETF were used (PDB accession number 4KPU (10)). Molecular graphics were produced using PyMOL (54). *Numbering* reflects *Rpa*FixAB amino acid sequence (UniProtKB accession numbers Q6N104 and Q6N105).

titration at pH 7, but future work should quantify proton uptake upon reduction of *Rpa*FixAB.

For $E^{\circ\prime}_{\text{ET-FAD, ASQ/HQ}}$, our value of −83 mV adjusted to pH 7 falls within the range of +25 to −197 (or lower) seen in the other ETFs. The 2-e$^-$ $E^{\circ\prime}$ of *Rpa*FixAB attributed to Bf-FAD is also comparable with that of *Mel*ETF, in agreement with the fact NADH reduces Bf-FAD directly in both (9). The absence of visible ASQ provides very valuable confirmation of the 2-e$^-$ nature of the transition, and the slightly depressed $E^{\circ\prime}$ relative to free FAD (57) demonstrates tuning on the part of the protein environment to minimize the energy dissipated by the hydride transfer from NADH to the Bf-flavin.

Based on our findings, we propose the following mechanism for *Rpa*FixAB-mediated electron bifurcation. With an $E^{\circ\prime}$ of −320 mV, NADH donates pairs of electrons as hydrides to Bf-FAD, which is tentatively assigned to the site where an FAD replaces the AMP of canonical ETFs (Fig. 9) (10). Our determination of an $E^{\circ\prime}$ of −223 mV confirms that such a transfer is favorable. Rapid transfer of an electron to the ET-FAD was proposed to require conformational change as the structure of isolated *Afe*ETF places the two flavins 18 Å apart (10). However, electron transfer could also exploit a hopping mechanism via the adenine of the Bf-FAD (58) and a conserved Tyr or Trp that distinguishes bifurcating ETFs from canonical ETFs (Tyr-37 in Fig. 9) (1). Tyr and Trp residues have been shown to mediate electron transfer over distances twice as large in ribonucleotide reductase, demonstrating their competence for such a role (59–62), which would also provide a satisfying rationale for the conservation of this residue specifically in bifurcating ETFs. Because the Bf-FAD has crossed potentials, transfer of one electron to the ET-FAD will produce a semiquinone state that is highly unstable and expected to rapidly reduce nearby acceptors. A recent study of FixABCX from *A. vinelandii* employed mass spectrometry in conjunction with crosslinking and molecular modeling to propose a structure of the assembly and suggests that FixX can bind immediately adjacent to the site attributed to Bf-FAD, placing a [4Fe-4S] cluster some 10 Å from the Bf-FAD (19). Such a close approach diminishes the necessity of conformational gating (12), as it allows that electron transfer to FixX can kinetically outcompete other more exergonic options, such as electron transfer to ET-FAD (35, 63).

ET-FAD need not be in the OX state that forms in contact with air, as intracellular milieu are generally much more reducing. Indeed, *Rpa*FixAB undergoes spontaneous reduction to the ASQ state of ET-FAD upon standing in inert atmosphere. If FixAB's resting state is ASQ at the ET-FAD site, then this flavin must cycle between its ASQ and HQ states, with the capacity to accept only one electron per turnover. Thus, the second electron from Bf-FAD would be constrained to pursue a different path ("bifurcation"), wherein the lower $E^{\circ\prime}$ of the ultimate electron acceptor, ferredoxin, would capture the energy inherent in the unstable Bf-FAD SQ. A mechanism allowing *only* a single electron per cycle to pass to the higher-potential acceptor constitutes the third requirement for bifurcation, along with a suppressed SQ state for the Bf-FAD and 1-e$^-$ transfer activity for the ET-FAD. Thus, our measured E° values obviate the need for any elaborate conformational changes to gate electron transfer, simplifying the mechanism and providing steps that can occur faster than the large-scale protein domain reorientations that had been thought be required (10).

The ET-FAD is proposed to transfer its acquired electron to quinones (Q) via FixC. At $E^{\circ\prime}_{\text{ET-FAD, ASQ/HQ}} = -83$ mV, this might appear to commit excessive driving force to this reaction. However, we propose that the FixC FAD accumulates two single electrons from two turnovers of FixAB, so the ET-FAD's $E^{\circ\prime}_{\text{ASQ/HQ}}$ needs to be lower than both of the E° values of FixC.

Whereas the above reaction is thermodynamically favorable overall, it rests on the transient participation of an unstable semiquinone of the Bf-FAD, which therefore cannot be observed in titrations (1, 12, 47, 48). Crucially, our TAS reveals ASQ species able to account for both flavins. As in other bifurcating systems investigated so far, TAS demonstrates that the transient semiquinone formed is anionic (47, 48). Indeed, coupled transfer of a proton to produce neutral semiquinone would be expected to stabilize it and slow the kinetics. However, in the case of *Rpa*FixAB, the lifetime of the photogenerated ASQ is longer than that of the bifurcating NADH-dependent ferredoxin:NADP$^+$ oxidoreductase I (NfnI) from *Pyrococcus furiosus* (47). This can be rationalized by the fact that FixAB lacks the partner proteins and supporting electron transfer chains that would normally be present to rapidly conduct the electron away from the ASQ (48). Although TAS of FixAB from *R. rubrum* revealed rapid ASQ decay in the absence of partner proteins, its FAD content was also notably lower than was achieved here (19). Thus, a substantial fraction of sites may have lacked charge separation ability, the electron acquired by the photoexcited flavin could have been drawn from a nearby

Trp or Tyr, and the donor-acceptor pair would undergo rapid charge recombination (48). In contrast, our *Rpa*FixAB contains both FADs in essentially every heterodimer, so photogenerated Bf-FAD ASQ may send its excess electron to ET-FAD via Tyr-37 (Fig. 9). Because this would produce a second species with essentially the same signal, it would be difficult to discern but would have a longer lifetime due to greater separation from the original donor.

In summary, our studies of this most recent addition to the group of two-FAD–containing ETFs have revealed distinct properties essential for flavin-based electron bifurcation. *Rpa*-FixAB's presumed Bf-FAD has a thermodynamically suppressed SQ, whereas the ET-FAD can provide efficient 1-e^- transfer away from the Bf-FAD upon its reduction. One could consider that bifurcation capacity in ETFs arose by evolution of the scaffold of canonical ETFs to acquire FAD binding at the AMP site. However, we propose instead that bifurcating ETFs may have existed first and that modern canonical ETFs represent a suppression of binding of the FMN portion of the Bf-FAD, which is not needed in the modern role. This loss would moreover have been favored by the Bf-FAD's tendency to produce reactive oxygen species and attendant stress upon exposure to O_2 (34). Thus, we imagine that before the great oxygenation event, anaerobic bacteria would have reaped the benefits of energy-conserving bifurcation mediated by bifurcating ETFs (64) but that the rise of O_2 and acquisition of respiratory capacity would have simultaneously provided new abundant energy sources rendering energy conservation less important to growth while also introducing the threat of oxidative stress. Thus, the Bf-FAD's susceptibility to oxidation by O_2 (34) would have become a liability. *Rpa*FixAB provides a rare and valuable opportunity to experimentally reproduce this proposed change and gain insights into how evolution of a one-FAD ETF could have occurred from a two-FAD starting point.

Compared with many other bifurcating systems involving Fe-S clusters, FixABCX is flavin-rich at its core. Fe-S clusters are carried by FixX, and the presumed quinone reductase FAD is in FixC. This modular architecture facilitates study of the individual components of the system. The central core of bifurcating FixABCX, FixAB, only contains flavin cofactors. Therefore, with our newly demonstrated capacity to separately monitor each of the two flavins by CD, FixAB is now a simple and ideal model for interrogating flavin-based electron bifurcation. Our studies on *Rpa*FixAB presented here have laid a foundation for more detailed elucidation of the mechanism and evolution of flavin-based bifurcation.

Experimental procedures

Cloning, overexpression, and purification of R. palustris FixAB

The gene sequences encoding FixA and FixB from *R. palustris* were PCR-amplified from genomic DNA of *R. palustris* CGA009 obtained from Caroline Harwood (University of Washington) with pairs of primers 5′-GTCTCTCCCATGCATATCGTCGTCTGTATCAAGCAGGTTCCG-3′/5′-GGTTCTCCCCAAATCCGCGCGCCAGCT-3′ and 5′-TACTTCCAATCCAATGCAATGAGCCAGCCCGCCAAGC-3′/5′-TTATCCACTTCCAATGCCTTAGCTCGCGATCCGGTCGC-3′, respectively. The genes were inserted using ligation-independent cloning into vectors acquired from the DNASU Plasmid Repository (Tempe, AZ), pMCSG28 for the expression of FixA and pMCSG21 for the expression of FixB. After DNA sequence verification (Eurofins Genomics, Louisville, KY), the *Escherichia coli* strain NiCo21(DE3) (New England Biolabs, Ipswich, MA) was transformed with both plasmids pMCSG28::*fixA* and pMCSG21::*fixB* to co-express *Rpa*FixAB. The expressed *Rpa*FixAB is expected to carry a C-terminal His tag on FixA and an N-terminal His tag on FixB to facilitate protein purification. Cells were grown in 6 liters of Terrific Broth supplemented with 20 mg/liter riboflavin and 2 mM $MgSO_4$ along with carbenicillin (100 μg/ml) and spectinomycin (100 μg/ml) at 37 °C, shaking at 200 rpm, to an OD_{600} of ~2. After fully cooling the culture to 18–20 °C, *fixAB* gene expression was induced with 0.1 mM isopropyl 1-thio-β-D-galactopyranoside, and cells were grown for an additional 12 h at this lower temperature. Cells were harvested by centrifugation at 11,899 × *g* at 4 °C for 6 min, and the pellet was stored at −80 °C.

Cell pellet was resuspended in 80 ml of BugBuster (EMD Millipore, Burlington, MA) containing 1 mM 4-(2-aminoethyl)benzenesulfonyl fluoride hydrochloride, 1 mM TCEP, 1 mM FAD, 20 μl of benzonase nuclease, and 2 μl of rLysozyme (EMD Millipore, Burlington, MA) and further incubated at 4 °C for 2 h with stirring. After centrifugation at 20,000 × *g* for 30 min at 4 °C, the supernatant was filtered through a 0.22-μm syringe filter. The resulting protein solution was mixed with 2.5 ml of pre-equilibrated nickel-nitrilotriacetic acid resin (EMD Millipore, Burlington, MA) and incubated overnight at 4 °C with stirring. The next day, the mixture was transferred to a column at 4 °C. After collecting the flow-through, the column was washed with 20 mM Tris, pH 7.8, 500 mM KCl, 10% (w/v) glycerol, and 1 mM TCEP containing 20 and 50 mM imidazole in sequence using 20 and 2 column volumes for each, respectively. Finally, the column was developed with 2 column volumes of 20 mM Tris, pH 7.8, 500 mM KCl, 10% (w/v) glycerol, and 1 mM TCEP containing 100 mM imidazole, and the eluate was collected in different fractions. After SDS-PAGE analysis, imidazole was removed from the pooled pure fractions by passage over a 10DG column (Bio-Rad) equilibrated with 20 mM Bistris propane, pH 9.0, 200 mM KCl, 10% (w/v) glycerol, and 1 mM TCEP. Any apoprotein was reconstituted by overnight incubation of the protein in 0.1 mM FAD at 4 °C. Excess flavin was then removed by gel filtration on a 10DG column (above) before prompt use or flash-freezing in liquid nitrogen and storage at −80 °C.

Flavin content quantification

Protein concentration was determined using the Pierce 660-nm protein assay with bovine serum albumin as the standard (Thermo Fisher Scientific, Waltham, MA). To quantify the flavin content, the protein sample was denatured by heating at 100 °C in the dark for 10 min. After cooling to 4 °C, the sample was centrifuged at 15,000 × *g* for 2 min to remove denatured proteins. The concentration of FAD in the supernatant was then quantified spectrophotometrically using the extinction coefficient $\epsilon_{450} = 11.3\ mM^{-1}\ cm^{-1}$ (65).

Protein identification by native mass spectrometry

Non-covalent mass spectrometry under native conditions was conducted on a SYNAPT G2-*Si* instrument (Waters Corp., Milford, MA), as described in detail previously (66). Briefly, the *Rpa*FixAB sample was buffer-exchanged with 200 mM ammonium acetate, pH 7.0, using a 3000-Da cutoff spin filter (Pall Corp., Port Washington, NY) and infused from in-house prepared gold-coated borosilicate glass capillaries to electrospray source at a protein concentration of 0.5 μM and a rate of ~90 nl/min. The instrument was tuned to enhance performance in the high mass-to-charge range. Settings were as follows: source temperature 30 °C, capillary voltage 1.7 kV, trap bias voltage 16 V, and argon flow in collision cell (trap) 7 ml/min. The transfer collision energy was held at 10 V, whereas trap energy varied between 10 and 200 V. Data analysis was performed in MassLynx software version 4.1 (Waters Corp.).

CD deconvolution of the two flavins in RpaFixAB

The two flavins of *Rpa*FixAB were deconvoluted by CD using two different approaches. In the first approach, the ET-FAD was dissociated from 65 μM protein by incubating with different concentrations of ATP (ϵ_{260} = 15.4 mM^{-1} cm^{-1}) (67) added in 3.25 mM increments at 4 °C. The UV-visible spectrum of the sample was recorded on a HP 8453 spectrophotometer (Agilent Technologies, Santa Clara, CA) at each ATP concentration using a 1-cm path length self-masking quartz cuvette with an airtight closed screw cap (Starna Cells, Atascadero, CA). After that, the CD spectrum was also recorded in a JASCO J-800 series spectropolarimeter from 600 to 300 nm at 4 °C with the following parameters: bandwidth = 2.00 nm, scanning speed = 100 nm/min, and accumulations = 4. The molar ellipticity [θ] can be calculated using the equation, $[\theta] = \theta/(c \times l)$, in which θ is the ellipticity in millidegrees, c is the concentration in mM, and l is the cell path length in cm. We note that attempting full displacement of FAD from one site by further increasing ATP concentration (to >13 mM) led to protein aggregation and that accurate quantification of released FAD proved difficult due to adsorption of FAD on the membrane of the centrifugal filter used for isolation of free FAD. Thus, a full-amplitude CD spectrum of the ET-FAD could not be obtained by this method. In support of the dominance of the nucleotide portion of FAD with respect to binding affinity, we found that *Rpa*FixAB did not bind FMN (data not shown).

In the second approach, the CD spectrum was monitored in the course of anaerobic reduction of *Rpa*FixAB (see below) by either NADH or sodium dithionite with the same spectropolarimeter parameters, except that for reduction by sodium dithionite, room temperature was used and with accumulations = 1.

Anaerobic titration of RpaFixAB by NADH and sodium dithionite

Anaerobic titrations were all monitored using a HP 8452A spectrophotometer (Agilent Technologies) equipped with an OLIS controller and housed in a Belle Technology (Weymouth, UK) glovebox (<1.8 ppm of oxygen) using a 1-cm path length self-masking quartz cuvette with an airtight closed screw cap (Starna Cells). 65 μM *Rpa*FixAB was titrated using NADH (ϵ_{340} = 6.22 mM^{-1} cm^{-1}) (68) in 32.5 μM increments at 4 °C or sodium dithionite (ϵ_{315} = 7.05 mM^{-1} cm^{-1}) (69) in 14.5 μM increments at room temperature.

Reduction midpoint potential determination of RpaFixAB

Potentiometric titrations were also performed in a HP 8452A spectrophotometer (Agilent Technologies) housed in a Belle Technology (Weymouth, UK) glovebox (<1.8 ppm of oxygen) using a 1-cm path length self-masking quartz cuvette with an airtight closed screw cap (Starna Cells) by the xanthine/xanthine oxidase electron delivery system (44). Each titration contained 400 μM xanthine, 1 μM methyl viologen, 10 μM *Rpa*FixAB, and the amount of the reference dye yielding absorbance comparable with that of the flavins of *Rpa*FixAB in 20 mM Bistris propane, pH 9.0, 200 mM KCl, 10% (w/v) glycerol, and 1 mM TCEP (70, 71). The reaction was initiated by the addition of a catalytic amount of xanthine oxidase (0.5–20 nM), and the spectral changes were monitored every 1 min. $E°$ values of *Rpa*FixAB were calculated from concurrent reduction of the reference dye and the specific flavin under investigation. To eliminate interference from the other flavin that presumably did not change, the difference spectra between the initial spectrum of each phase (see below) and the observed spectra in the course of reduction were used, and simultaneous equations were developed to account for conversion to the reduced states of flavin and dye in each reduction phase (72). The following extinction coefficients were used: $\Delta\epsilon_{456}$(ET-FAD$_{OX\text{-}SQ}$) = 6.57 mM^{-1} cm^{-1}, $\Delta\epsilon_{456}$(ET-FAD$_{SQ\text{-}HQ}$) = 4.03 mM^{-1} cm^{-1}, and $\Delta\epsilon_{456}$ (Bf-FAD$_{OX\text{-}HQ}$) = 9.17 mM^{-1} cm^{-1}) (Fig. S3). Linear regression analysis of ln([FAD$_{OX}$]/[FAD$_{RED}$]) *versus* ln([Dye$_{OX}$]/[Dye$_{RED}$]) was performed using GraphPad Prism version 7.0a for Mac OS X (GraphPad Software, La Jolla, CA), and fit to Equation 1.

$$\ln\left(\frac{[F_{OX}]}{[F_{RED}]}\right) = b + \frac{n_F}{n_D}\ln\left(\frac{[D_{OX}]}{[D_{RED}]}\right) \quad \text{(Eq. 1)}$$

where [F$_{OX}$] is the concentration of the reacting flavin in the oxidized state, [F$_{RED}$] is the concentration in the state formed upon reduction, [D$_{OX}$] and [D$_{RED}$] have the same meanings for the dye, n_F and n_D denote the number of electrons acquired by the flavin and the dye, respectively, in the reaction under study, and b is the intercept produced by the fit.

The value obtained for b was then used with the midpoint potential of the dye, $E°_D$, to calculate that of the flavin, $E°_F$, using Equation 2,

$$b = \frac{n_F}{25.7\ \text{mV}}(E°_D - E°_F) \quad \text{(Eq. 2)}$$

where 25.7 mV replaces RT/F (ideal gas constant times absolute temperature divided by Faraday's constant).

All potentials are reported relative to the normal hydrogen electrode and represent the average of three independent determinations. Because the titrations were conducted at pH 9.0, the reported values for pH 7.0 in Table 1 were calculated based on the assumptions that $E°$ does not change with pH when no proton transfer is involved in the reduction ($E°_{OX/ASQ}$); $E°$ is decreased by 60 mV with every one-pH unit increase when

acquisition of one proton accompanies 1-e$^-$ reduction ($E^\circ_{ASQ/HQ}$); E° decreases by 30 mV per unit increase in pH for the reduction of Bf-FAD, assuming this to be one proton/two electrons at pH 9.0 ($E^\circ_{OX/HQ}$). The extinction coefficients and E° values (73) of the reference dyes used are as follows: methylene blue ($\epsilon_{664} = 76\ mM^{-1}\ cm^{-1}$, $E^{\circ\prime} = +11$ mV, calc. E° at pH 9 of −49 mV) (74), Nile blue ($\epsilon_{636} = 27\ mM^{-1}\ cm^{-1}$, $E^{\circ\prime} = -116$ mV, calc. E° at pH 9 of −236 mV) (75) and phenosafranin ($\epsilon_{520} = 29\ mM^{-1}\ cm^{-1}$, $E^{\circ\prime} = -252$ mV, calc. E° at pH 9 of −312 mV) (76).

Transient absorption spectroscopy

The ultrafast (100 fs to 5.1 ns) TAS spectrometer employed in this study uses an amplified 4W Ti:sapphire laser (Libra, Coherent, 800 nm, 1 kHz, 100-fs pulse width), and the Helios spectrometer (Ultrafast Systems, LLC, Sarasota, FL). A fraction of the 800-nm Libra output was frequency-doubled in β barium borate (BBO) to produce the desired pump wavelength (400 nm) for sample excitation, which was then directed into the Helios. The pump pulses were passed through a depolarizer and chopped by a synchronized chopper to 500 Hz before reaching the sample. The pump pulse energy was 1.1 μJ/pulse at the sample. Another fraction of the 800-nm Libra output was guided directly into the Helios for generation of the probe. Within the spectrometer, a white light continuum of wavelengths including 340–800 nm was generated using a 2-mm thick CaF_2 crystal. This beam was split into a probe beam and a reference beam. The probe beam was focused into the sample, where it was overlapped with the pump beam. The transmitted probe and reference beams were then focused into optical fibers coupled to multichannel spectrometers with CMOS (complementary metal-oxide-semiconductor) sensors with 1-kHz detection rates. The reference signal is used to correct the probe signal for pulse-to-pulse fluctuations in the white-light continuum. The time delay between the pump and probe pulses was controlled by a motorized delay stage.

For all transient absorption measurements, the sample was made in an MBraun glovebox (N_2 atmosphere), sealed in a 2-mm quartz cuvette, and constantly stirred to prevent photodegradation. The protein concentration of *Rpa*FixAB used was 133 μM, and it was characterized in its as-isolated state (oxidized). For the purpose of this study, light initiated the formation of the semiquinone intermediates for each flavin through generation of FAD excited state and electron donation from nearby protein residues or the other flavin. Qualitatively, this experiment shows which type of semiquinone is formed for a particular FAD site and suggests how thermodynamically stable that intermediate is, based on its lifetime. All experiments were conducted at room temperature. The change in absorbance signal (ΔA) was calculated from the intensities of signals detected after sequential probe pulses with and without the pump pulse excitation. The data collection (350 pump shots per time point) was carried out three consecutive times and then averaged. Data were corrected for spectral chirp using SurfaceXplorer (Ultrafast Systems, LLC, Sarasota, FL). ASQ signals were fit in IGOR Pro (WaveMetrics) with a double-exponential function.

Author contributions—H. D. D., C. E. L., M. T. -L., P. W. K., J. W. P., and A. -F. M. conceptualization; P. W. K., J. W. P., and A. -F. M. resources; H. D. D., C. E. L., M. T. -L., and G. H. G. data curation; H. D. D., C. E. L., M. T. -L., G. H. G., and A. -F. M. software; H. D. D., C. E. L., M. T. -L., G. H. G., and A. -F. M. formal analysis; H. D. D., B. B., P. W. K., J. W. P., and A. -F. M. supervision; H. D. D., B. B., P. W. K., J. W. P., and A. -F. M. funding acquisition; H. D. D., C. E. L., M. T. -L., G. H. G., B. B., P. W. K., J. W. P., and A. -F. M. validation; H. D. D., C. E. L., M. T. -L., G. H. G., and B. B. investigation; H. D. D., C. E. L., M. T. -L., G. H. G., B. B., P. W. K., and A. -F. M. methodology; H. D. D. and C. E. L. writing-original draft; H. D. D., B. B., P. W. K., J. W. P., and A. -F. M. project administration; H. D. D., C. E. L., M. T. -L., G. H. G., B. B., P. W. K., J. W. P., and A. -F. M. writing-review and editing.

Acknowledgments—We thank Professor Caroline Harwood (University of Washington) for the gift of R. palustris genomic DNA, Professor Edith Glazer (University of Kentucky) for the access to a high-capacity centrifuge, and the Montana State University Microfabrication Facility for help in preparation of gold-coated borosilicate glass capillaries for non-covalent mass spectrometry. We thank Rhesa Ledbetter, Amaya Garcia Costas, and Gerrit Schut for insightful conversations. A. F. M. acknowledges the hospitality of the Technische Universität-Berlin and the support of UNICAT during the revision of the manuscript. The Proteomics, Metabolomics, and Mass Spectrometry Facility at Montana State University has received support from the Murdock Charitable Trust and NIGMS, National Institutes of Health, under Grant P20GM103474.

Addendum—Since submission of the current manuscript, a report has been published demonstrating that large-scale conformational changes accompanying binding of partner protein result in greatly shortened flavin-to-flavin distances that can support rapid direct electron transfer between them in another electron transfer flavoprotein. That excellent work also reaches the same conclusion as we do regarding the states of the ET-FAD that participate in turnover, as per a reviewer's comment. The reader is referred to Demmer *et al.* (77).

References

1. Garcia Costas, A. M., Poudel, S., Miller, A.-F., Schut, G. J., Ledbetter, R. N., Fixen, K. R., Seefeldt, L. C., Adams, M. W. W., Harwood, C. S., Boyd, E. S., and Peters, J. W. (2017) Defining electron bifurcation in the electron transferring flavoprotein family. *J. Bacteriol.* **199,** e00440-17 Medline
2. Toogood, H. S., Leys, D., and Scrutton, N. S. (2007) Dynamics driving function : new insights from electron transferring flavoproteins and partner complexes. *FEBS J.* **274,** 5481–5504 CrossRef Medline
3. Watmough, N. J., and Frerman, F. E. (2010) The electron transfer flavoprotein: ubiquinone oxidoreductases. *Biochim. Biophys. Acta* **1797,** 1910–1916 CrossRef Medline
4. Frerman, F. E., and Goodman, S. I. (1985) Deficiency of electron transfer flavoprotein or electron transfer flavoprotein:ubiquinone oxidoreductase in glutaric acidemia type II fibroblasts. *Proc. Natl. Acad. Sci. U.S.A.* **82,** 4517–4520 CrossRef Medline
5. Henriques, B. J., Bross, P., and Gomes, C. M. (2010) Mutational hotspots in electron transfer flavoprotein underlie defective folding and function in multiple acyl-CoA dehydrogenase deficiency. *Biochim. Biophys. Acta* **1802,** 1070–1077 CrossRef Medline
6. Sato, K., Nishina, Y., and Shiga, K. (1993) Electron-transferring flavoprotein has an AMP-binding site in addition to the FAD-binding site. *J. Biochem.* **114,** 215–222 CrossRef Medline
7. Sato, K., Nishina, Y., and Shiga, K. (1996) *In vitro* refolding and unfolding of subunits of electron-transferring flavoprotein: characterization of the folding intermediates and the effects of FAD and AMP on the folding reaction. *J. Biochem.* **120,** 276–285 CrossRef Medline

8. DuPlessis, E. R., Rohlfs, R. J., Hille, R., and Thorpe, C. (1994) Electron-transferring flavoproteins from pig and the methylotrophic bacterium W3A1 contains AMP as well as FAD. *Biochem. Mol. Biol. Int.* **32,** 195–199 Medline
9. Sato, K., Nishina, Y., and Shiga, K. (2013) Interaction between NADH and electron-transferring flavoprotein from *Megasphaera elsdenii*. *J. Biochem.* **153,** 565–572 CrossRef Medline
10. Chowdhury, N. P., Mowafy, A. M., Demmer, J. K., Upadhyay, V., Koelzer, S., Jayamani, E., Kahnt, J., Hornung, M., Demmer, U., Ermler, U., and Buckel, W. (2014) Studies on the mechanism of electron bifurcation catalyzed by electron transferring flavoprotein (Etf) and butyryl-CoA dehydrogenase (Bcd) of Acidaminococcus fermentans. *J. Biol. Chem.* **289,** 5145–5157 CrossRef Medline
11. Sato, K., Nishina, Y., and Shiga, K. (2003) Purification of electron-transferring flavoprotein from Megasphaera elsdenii and binding of additional FAD with an unusual absorption spectrum. *J. Biochem.* **134,** 719–729 CrossRef Medline
12. Peters, J. W., Miller, A. F., Jones, A. K., King, P. W., and Adams, M. W. (2016) Electron bifurcation. *Curr. Opin. Chem. Biol.* **31,** 146–152 CrossRef Medline
13. Rodkey, F. L. (1955) Oxidation-reduction potentials of the diphosphopyridine nucleotide system. *J. Biol. Chem.* **213,** 777–786 Medline
14. Tagawa, K., and Arnon, D. I. (1968) Oxidation-reduction potentials and stoichiometry of electron transfer in ferredoxins. *Biochim. Biophys. Acta* **153,** 602–613 CrossRef Medline
15. Chowdhury, N. P., Klomann, K., Seubert, A., and Buckel, W. (2016) Reduction of flavodoxin by electron bifurcation and sodium ion-dependent reoxidation by NAD^+ catalyzed by ferredoxin-NAD^+ reductase (Rnf). *J. Biol. Chem.* **291,** 11993–12002 CrossRef Medline
16. Huang, J. J., Heiniger, E. K., McKinlay, J. B., and Harwood, C. S. (2010) Production of hydrogen gas from light and the inorganic electron donor thiosulfate by *Rhodopseudomonas palustris*. *Appl. Environ. Microbiol.* **76,** 7717–7722 CrossRef Medline
17. Earl, C. D., Ronson, C. W., and Ausubel, F. M. (1987) Genetic and structural analysis of the *Rhizobium meliloti* fixA, fixB, fixC, and fixX genes. *J. Bacteriol.* **169,** 1127–1136 CrossRef Medline
18. Edgren, T., and Nordlund, S. (2004) The *fixABCX* genes in *Rhodospirillum rubrum* encode a putative membrane complex participating in electron transfer to nitrogenase. *J. Bacteriol.* **186,** 2052–2060 CrossRef Medline
19. Ledbetter, R. N., Garcia Costas, A. M., Lubner, C. E., Mulder, D. W., Tokmina-Lukaszewska, M., Artz, J. H., Patterson, A., Magnuson, T. S., Jay, Z. J., Duan, H. D., Miller, J., Plunkett, M. H., Hoben, J. P., Barney, B. M., Carlson, R. P., *et al.* (2017) The electron bifurcating FixABCX protein complex from *Azotobacter vinelandii*: generation of low-potential reducing equivalents for nitrogenase catalysis. *Biochemistry* **56,** 4177–4190 CrossRef Medline
20. Westphal, A. H., Swaving, J., Jacobs, L., and De Kok, A. (1998) Purification and characterization of a flavoprotein involved in the degradation of epoxyalkanes by *Xanthobacter* Py2. *Eur. J. Biochem.* **257,** 160–168 CrossRef Medline
21. Williams, C. H. J. (1992) in *Chemistry and biochemistry of flavoenzymes* (Müller, F., ed) pp. 121–211, CRC Press, Inc., Boca Raton, FL
22. Gadda, G., Edmondson, R. D., Russell, D. H., and Fitzpatrick, P. F. (1997) Identification of the naturally occurring flavin of nitroalkane oxidase from fusarium oxysporum as a 5-nitrobutyl-FAD and conversion of the enzyme to the active FAD-containing form. *J. Biol. Chem.* **272,** 5563–5570 CrossRef Medline
23. Kirchner, U., Westphal, A. H., Müller, R., and van Berkel, W. J. (2003) Phenol hydroxylase from *Bacillus thermoglucosidasius* A7, a two-protein component monooxygenase with a dual role for FAD. *J. Biol. Chem.* **278,** 47545–47553 CrossRef Medline
24. Salazar, D., Zhang, L., deGala, G. D., and Frerman, F. E. (1997) Expression and characterization of two pathogenic mutations in human electron transfer flavoprotein. *J. Biol. Chem.* **272,** 26425–26433 CrossRef Medline
25. Herrick, K. R., Salazar, D., Goodman, S. I., Finocchiaro, G., Bedzyk, L. A., and Frerman, F. E. (1994) Expression and characterization of human and chimeric human-*Paracoccus denitrificans* electron transfer flavoproteins. *J. Biol. Chem.* **269,** 32239–32245 Medline
26. Sato, K., Nishina, Y., and Shiga, K. (1992) The binding of adenine nucleotides to apo-electron-transferring flavoprotein. *J. Biochem.* **112,** 804–810 CrossRef Medline
27. Byron, C. M., Stankovich, M. T., Husain, M., and Davidson, V. L. (1989) Unusual redox properties of electron-transfer flavoprotein from *Methylophilus methylotrophus*. *Biochemistry* **28,** 8582–8587 CrossRef Medline
28. Wilson, E. K., Huang, L., Sutcliffe, M. J., Mathews, F. S., Hille, R., and Scrutton, N. S. (1997) An exposed tyrosine on the surface of trimethylamine dehydrogenase facilitates electron transfer to electron transferring flavoprotein: kinetics of transfer in wild-type and mutant complexes. *Biochemistry* **36,** 41–48 CrossRef Medline
29. Talfournier, F., Munro, A. W., Basran, J., Sutcliffe, M. J., Daff, S., Chapman, S. K., and Scrutton, N. S. (2001) α Arg-237 in *Methylophilus methylotrophus* (sp. W3A1) electron-transferring flavoprotein affords approximately 200-millivolt stabilization of the FAD anionic semiquinone and a kinetic block on full reduction to the dihydroquinone. *J. Biol. Chem.* **276,** 20190–20196 CrossRef Medline
30. Dwyer, T. M., Zhang, L., Muller, M., Marrugo, F., and Frerman, F. (1999) The functions of the flavin contact residues, αArg249 and βTyr16, in human electron transfer flavoprotein. *Biochim. Biophys. Acta* **1433,** 139–152 CrossRef Medline
31. Gustafson, W. G., Feinberg, B. A., and McFarland, J. T. (1986) Energetics of β-oxidation: reduction potentials of general fatty acyl-CoA dehydrogenase, electron transfer flavoprotein, and fatty acyl-CoA substrates. *J. Biol. Chem.* **261,** 7733–7741 Medline
32. Husain, M., Stankovich, M. T., and Fox, B. G. (1984) Measurement of the oxidation-reduction potentials for one-electron and two-electron reduction of electron-transfer flavoprotein from pig liver. *Biochem. J.* **219,** 1043–1047 CrossRef Medline
33. Husain, M., and Steenkamp, D. J. (1983) Electron transfer flavoprotein from pig liver mitochondria: a simple purification and re-evaluation of some of the molecular properties. *Biochem. J.* **209,** 541–545 CrossRef Medline
34. Chowdhury, N. P., Kahnt, J., and Buckel, W. (2015) Reduction of ferredoxin or oxygen by flavin-based electron bifurcation in *Megasphaera elsdenii*. *FEBS J.* **282,** 3149–3160 CrossRef Medline
35. Nitschke, W., and Russell, M. J. (2012) Redox bifurcations: mechanisms and importance to life now, and at its origin: a widespread means of energy conversion in biology unfolds. *BioEssays* **34,** 106–109 CrossRef Medline
36. Demmer, J. K., Huang, H., Wang, S., Demmer, U., Thauer, R. K., and Ermler, U. (2015) Insights into flavin-based electron bifurcation via the NADH-dependent reduced ferredoxin:NADP oxidoreductase structure. *J. Biol. Chem.* **290,** 21985–21995 CrossRef Medline
37. Lin, T.-Y., Werther, T., Jeoung, J.-H., and Dobbek, H. (2012) Suppression of electron transfer to dioxygen by charge transfer and electron transfer complexes in the FAD-dependent reductase component of toluene dioxygenase. *J. Biol. Chem.* **287,** 38338–38346 CrossRef Medline
38. Sakurai, T., and Hosoya, H. (1966) Charge-transfer complexes of nicotinamide-adenine dinucleotide analogues and flavin mononucleotide. *Biochim. Biophys. Acta* **112,** 459–468 CrossRef
39. Abramovitz, A. S., and Massey, V. (1976) Interaction of phenols with old yellow enzyme: physical evidence for charge-transfer complexes. *J. Biol. Chem.* **251,** 5327–5336 Medline
40. Hay, S., Pudney, C. R., McGrory, T. A., Pang, J., Sutcliffe, M. J., and Scrutton, N. S. (2009) Barrier compression enhances an enzymatic hydrogen-transfer reaction. *Angew. Chem. Int. Ed. Engl.* **48,** 1452–1454 CrossRef Medline
41. Miller, S. M., Massey, V., Ballou, D., Williams, C. H., Jr., Distefano, M. D., Moore, M. J., and Walsh, C. T. (1990) Use of a site-directed triple mutant to trap intermediates: demonstration that the flavin C(4a)-thiol adduct and reduced flavin are kinetically competent intermediates in mercuric ion reductase. *Biochemistry* **29,** 2831–2841 CrossRef Medline
42. Pudney, C. R., Hay, S., Pang, J., Costello, C., Leys, D., Sutcliffe, M. J., and Scrutton, N. S. (2007) Mutagenesis of morphinone reductase induces multiple reactive configurations and identifies potential ambiguity in kinetic analysis of enzyme tunneling mechanisms. *J. Am. Chem. Soc.* **129,** 13949–13956 CrossRef Medline

43. Geng, J., Dornevil, K., Davidson, V. L., and Liu, A. (2013) Tryptophan-mediated charge-resonance stabilization in the bis-Fe(IV) redox state of MauG. *Proc. Natl. Acad. Sci. U.S.A.* **110,** 9639–9644 CrossRef Medline
44. Massey, V. (1991) A simple method for determination of redox potentials. in *Flavins and Flavoproteins* (Curti, B., Ronchi, S., and Zanetti, G., eds) pp. 59–66, Walter de Gruyer, Berlin
45. Dutton, P. L. (1978) Redox potentiometry: determination of midpoint potentials of oxidation-reduction components of biological electron-transfer systems. *Methods Enzymol.* **54,** 411–435 CrossRef Medline
46. Yang, K. Y., and Swenson, R. P. (2007) Modulation of the redox properties of the flavin cofactor through hydrogen-bonding interactions with the N(5) atom: role of α Ser254 in the electron-transfer flavoprotein from the methylotrophic bacterium W3A1. *Biochemistry* **46,** 2289–2297 CrossRef Medline
47. Lubner, C. E., Jennings, D. P., Mulder, D. W., Schut, G. J., Zadvornyy, O. A., Hoben, J. P., Tokmina-Lukaszewska, M., Berry, L., Nguyen, D. M., Lipscomb, G. L., Bothner, B., Jones, A. K., Miller, A. F., King, P. W., Adams, M. W. W., and Peters, J. W. (2017) Mechanistic insights into energy conservation by flavin-based electron bifurcation. *Nat. Chem. Biol.* **13,** 655–659 CrossRef Medline
48. Hoben, J. P., Lubner, C. E., Ratzloff, M. W., Schut, G. J., Nguyen, D. M. N., Hempel, K. W., Adams, M. W. W., King, P. W., and Miller, A. F. (2017) Equilibrium and ultrafast kinetic studies manipulating electron transfer: a short-lived flavin semiquinone is not sufficient for electron bifurcation. *J. Biol. Chem.* **292,** 14039–14049 CrossRef Medline
49. Mataga, N., Chosrowjan, H., Taniguchi, S., Tanaka, F., Kido, N., and Kitamura, M. (2002) Femtosecond fluorescence dynamics of flavoproteins: comparative studies on flavodoxin, its site-directed mutants, and riboflavin binding protein regarding ultrafast electron transfer in protein nanospaces. *J. Phys. Chem. B* **106,** 8917–8920 CrossRef
50. Mathes, T., van Stokkum, I. H. M., Stierl, M., and Kennis, J. T. M. (2012) Redox modulation of flavin and tyrosine determines photoinduced proton-coupled electron transfer and photoactivation of BLUF photoreceptors. *J. Biol. Chem.* **287,** 31725–31738 CrossRef Medline
51. Hardman, S. J. O., Pudney, C. R., Hay, S., and Scrutton, N. S. (2013) Excited state dynamics can be used to probe donor-acceptor distances for H-tunneling reactions catalized by flavoproteins. *Biophys. J.* **105,** 2549–2558 CrossRef Medline
52. Enescu, M., Lindqvist, L., and Soep, B. (1998) Excited-state dynamics of fully reduced flavins and flavoenzymes studied at subpicosecond time resolution. *Photochem. Photobiol.* **68,** 150–156 CrossRef Medline
53. Morrison, E., Kantz, A., Gassner, G. T., and Sazinsky, M. H. (2013) Structure and mechanism of styrene monooxygenase reductase: new insight into the FAD-transfer reaction. *Biochemistry* **52,** 6063–6075 CrossRef Medline
54. Yang, C.-Y. (2006) *The Effects of the N(5) Hydrogen Bond and the Re-face Positive Charge on the Redox Properties of Flavin in the Methylotrophic Bacterium W3A1 Electron Transfer Flavoprotein*, Ph.D. thesis, Ohio State University, Columbus, Ohio
55. Griffin, K. J., Dwyer, T. M., Manning, M. C., Meyer, J. D., Carpenter, J. F., and Frerman, F. E. (1997) αT244M mutation affects the redox, kinetic, and *in vitro* folding properties of *Paracoccus denitrificans* electron transfer flavoprotein. *Biochemistry* **36,** 4194–4202 CrossRef Medline
56. Roberts, D. L., Salazar, D., Fulmer, J. P., Frerman, F. E., and Kim, J. J. (1999) Crystal structure of *Paracoccus denitrificans* electron transfer flavoprotein: structural and electrostatic analysis of a conserved flavin binding domain. *Biochemistry* **38,** 1977–1989 CrossRef Medline
57. Mayhew, S. G. (1999) The effects of pH and semiquinone formation on the oxidation-reduction potentials of flavin mononucleotide: a reappraisal. *Eur. J. Biochem.* **265,** 698–702 CrossRef Medline
58. Liu, Z., Guo, X., Tan, C., Li, J., Kao, Y.-T., Wang, L., Sancar, A., and Zhong, D. (2012) Electron tunneling pathways and role of adenine in repair of cyclobutane pyrimidine dimer by DNA photolyase. *J. Am. Chem. Soc.* **134,** 8104–8114 CrossRef Medline
59. Gray, H. B., and Winkler, J. R. (2015) Hole hopping through tyrosine/tryptophan chains protects proteins from oxidative damage. *Proc. Natl. Acad. Sci. U.S.A.* **112,** 10920–10925 CrossRef Medline
60. Warren, J. J., Ener, M. E., Vlček, A., Jr., Winkler, J. R., and Gray, H. B. (2012) Electron hopping through proteins. *Coord. Chem. Rev.* **256,** 2478–2487 CrossRef Medline
61. Yee, C. S., Chang, M. C. Y., Ge, J., Nocera, D. G., and Stubbe, J. (2003) 2,3-Difluorotyrosine at position 356 of ribonucleotide reductase R2: a probe of long-range proton-coupled electron transfer. *J. Am. Chem. Soc.* **125,** 10506–10507 CrossRef Medline
62. Seyedsayamdost, M. R., Xie, J., Chan, C. T., Schultz, P. G., and Stubbe, J. (2007) Site-specific insertion of 3-aminotyrosine into subunit α2 of *E. coli* ribonucleotide reductase: direct evidence for involvement of Y730 and Y731 in radical propagation. *J. Am. Chem. Soc.* **129,** 15060–15071 CrossRef Medline
63. Zhang, P., Yuly, J. L., Lubner, C. E., Mulder, D. W., King, P. W., Peters, J. W., and Beratan, D. N. (2017) Electron bifurcation: thermodynamics and kinetics of two-electron brokering in biological redox chemistry. *Acc. Chem. Res.* **50,** 2410–2417 CrossRef Medline
64. Herrmann, G., Jayamani, E., Mai, G., and Buckel, W. (2008) Energy conservation via electron-transferring flavoprotein in anaerobic bacteria. *J. Bacteriol.* **190,** 784–791 CrossRef Medline
65. Whitby, L. G. (1953) A new method for preparing flavin-adenine dinucleotide. *Biochem. J.* **54,** 437–442 CrossRef Medline
66. Luo, M. L., Jackson, R. N., Denny, S. R., Tokmina-Lukaszewska, M., Maksimchuk, K. R., Lin, W., Bothner, B., Wiedenheft, B., and Beisel, C. L. (2016) The CRISPR RNA-guided surveillance complex in *Escherichia coli* accommodates extended RNA spacers. *Nucleic Acids Res.* **44,** 7385–7394 Medline
67. Bock, R. M., Ling, N. S., Morell, S. A., and Lipton, S. H. (1956) Ultraviolet absorption spectra of adenosine-5′-triphosphate and related 5′-ribonucleotides. *Arch. Biochem. Biophys.* **62,** 253–264 CrossRef Medline
68. Haid, E., Lehmann, P., and Ziegenhorn, J. (1975) Molar absorptivities of β-NADH and β-NAD at 260 nm. *Clin. Chem.* **21,** 884–887 Medline
69. Mayhew, S. G. (1978) The redox potential of dithionite and SO-2 from equilibrium reactions with flavodoxins, methyl viologen and hydrogen plus hydrogenase. *Eur. J. Biochem.* **85,** 535–547 CrossRef Medline
70. Mishanina, T. V., Yadav, P. K., Ballou, D. P., and Banerjee, R. (2015) Transient kinetic analysis of hydrogen sulfide oxidation catalyzed by human sulfide quinone oxidoreductase. *J. Biol. Chem.* **290,** 25072–25080 CrossRef Medline
71. Efimov, I., Parkin, G., Millett, E. S., Glenday, J., Chan, C. K., Weedon, H., Randhawa, H., Basran, J., and Raven, E. L. (2014) A simple method for the determination of reduction potentials in heme proteins. *FEBS Lett.* **588,** 701–704 CrossRef Medline
72. Trimmer, E. E., Ballou, D. P., Galloway, L. J., Scannell, S. A., Brinker, D. R., and Casas, K. R. (2005) Aspartate 120 of *Escherichia coli* methylenetetrahydrofolate reductase: evidence for major roles in folate binding and catalysis and a minor role in flavin reactivity. *Biochemistry* **44,** 6809–6822 CrossRef Medline
73. Clark, W. M. (1960) *Oxidation-Reduction Potentials of Organic Systems*, Williams and Wilkins, Baltimore
74. Nordén, B., and Tjerneld, F. (1982) Structure of methylene blue-DNA complexes studied by linear and circular dichroism spectroscopy. *Biopolymers* **21,** 1713–1734 CrossRef Medline
75. O'Reilly, J. P., Butts, C. P., l'Anson, I. A., and Shaw, A. M. (2005) Interfacial pH at an isolated silica-water surface. *J. Am. Chem. Soc.* **127,** 1632–1633 CrossRef Medline
76. Wang, J., Krizowski, S., Fischer-Schrader, K., Niks, D., Tejero, J., Sparacino-Watkins, C., Wang, L., Ragireddy, V., Frizzell, S., Kelley, E. E., Zhang, Y., Basu, P., Hille, R., Schwarz, G., and Gladwin, M. T. (2015) Sulfite oxidase catalyzes single-electron transfer at molybdenum domain to reduce nitrite to nitric oxide. *Antioxid. Redox Signal.* **23,** 283–294 CrossRef Medline
77. Demmer, J. K., Chowdhury, N. P., Selmer, T., Ermler, U., and Buckel, W. (2018) The semiquinone swing in the bifurcating electron transferring flavoprotein/butyryl-CoA dehydrogenase complex from *Clostridium difficile*. *Nat. Commun.* 10.1038/s41467-017-01746-3 CrossRef

Distinct properties underlie flavin-based electron bifurcation in a novel electron transfer flavoprotein FixAB from *Rhodopseudomonas palustris*

H. Diessel Duan, Carolyn E. Lubner, Monika Tokmina-Lukaszewska, George H. Gauss, Brian Bothner, Paul W. King, John W. Peters and Anne-Frances Miller

J. Biol. Chem. 2018, 293:4688-4701.
doi: 10.1074/jbc.RA117.000707 originally published online February 9, 2018
